Vilnius
University
Press

Pulsating flow and heat transfer of power-law fluid in a circular pipe

Ayse Nur Altunkaya[a] , **Orhan Aydin**[b,1] , **Mete Avci**[a]

[a]Department of Mechanical Engineering,
Recep Tayyip Erdogan University,
53100 Rize, Türkiye

[b]Department of Mechanical Engineering,
Karadeniz Technical University,
61080 Trabzon, Türkiye
oaydin@ktu.edu.tr

Abstract. In this study, the pulsating flow of a non-Newtonian fluid and heat transfer in a pipe with uniform heat flux at its wall is examined analytically. The flow is assumed to be both hydrodynamically and thermally fully developed. The perturbation method based on the series expansion is used in the analysis. The periodic change and period-averaged values of the friction factor and Nusselt number as well as velocity and temperature profiles are obtained at varying values of dimensionless frequency and amplitude for shear-thinning, Newtonian and shear-thickening fluids. It is shown that the frequency is effective on the friction factor for a specific range of the dimensionless frequency. For some specific cases, excellent agreements are obtained with the literature. It is disclosed that the dimensionless frequency, the amplitude and the power-law index are interactively effective on the friction and heat transfer.

Keywords: pulsating flow, pipe, power-law fluid, heat transfer.

1 Introduction

Understanding the characteristics of pulsating flow in closed channels is of noteworthy interest in many areas of engineering and general applications. Examples that may be given in this concept include respiratory and circulatory systems (blood flow in the main arteries and capillaries), fluid movement in biological chips used in disease diagnosis, bioreactor systems, cleaning-in-place systems, thermoacoustic systems, cooling systems of nuclear reactors and internal combustion engines along with hydraulic and pneumatic control systems.

In general, the pulsating flow is a specific type of unsteady flow consisting of steady and superimposed oscillating flow components. In this flow type, the amplitude and frequency of the oscillation play a critical role on the development and thickness of boundary layer, which can significantly change the flow resistance and heat transfer characteristics.

The pulsating flow problem in straight ducts of constant section has been widely studied by researchers for both laminar and turbulent flow regimes. However, because of the complexity of modeling/solving procedures, the fluid is generally assumed as Newtonian with constant properties in most of these theoretical studies. In a pioneering work of [25], the oscillating flow of Newtonian fluid in a straight pipe was solved analytically under fully developed laminar flow condition. It was concluded that the phase lag between the oscillating pressure and the flow tended to be $0°$ at low values of frequency, while it was approaching to $90°$ with an asymptotic increase at higher values. Uchida [23] analytically investigated the effect of frequency on both the velocity field and shear stress in a laminar pulsating pipe flow. The author reported that the fully developed velocity profile showed a significant change by taking an annular form in high frequency ranges, while it was maintaining its parabolic shape in low frequency ranges. Siegel and Perlmutter [22] conducted an analytical study to examine the heat transfer characteristics of pulsating flow between two-dimensional parallel plates exposed to the constant wall temperature. Their results indicated that the total heat transfer was not changed by the oscillation remarkably. Cho and Hyun [10] modeled both pulsating flow characteristics and heat transfer behavior of Newtonian fluid in a pipe by using boundary layer equations. They found out that the pulsating flow enhanced the heat transfer rate in a moderate frequency range; meanwhile, it had an opposite effect at very high and low frequencies compared to steady flow. Moschandreou and Zamir [19] considered the problem of pulsating flow in a circular tube with constant heat flux thermal boundary condition. By using the Green's function method, they derived analytical expressions both for the fully developed temperature profile and Nusselt number. They reported that the pulsation had an aiding effect on the heat transfer in the moderate values of frequency ($1-2$ Hz), while an opposite trend was observed the moment the frequency was out of this range. Readers are referred to see reviews related to pulsating flow of Newtonian fluid in common conduits by Carpinlioglu and Gündogdu [8]. Yu et al. [16] analyzed the effects of dimensionless frequency, amplitude and Prandtl number on the heat transfer characteristics of laminar pulsating flow in a circular conduit. In a study in a similar vein, Nield and Kuznetsov [20] analytically solved the forced convection problem in both parallel-plate and circular channels by using the perturbation method. On the other hand, Craciunescu and Clegg [11] numerically investigated the effect of blood velocity pulsations on heat transfer within four blood vessels, which were the aorta, large arteries, arterioles and terminal arterial branches by assuming the blood as a Newtonian fluid. In another study, Yan et al. [26] theoretically studied the effects of Prandtl number, oscillating amplitude and rolling frequency on the Nusselt number in a pipe. They found that the oscillation amplitude of the Nusselt number was increased with the increase of Prandtl number. As a further remark, Aygun and Aydin [3, 4] carried out experimental, numerical and analytical studies to examine the role of pulsation frequency on the friction coefficient in both developing and fully developed piston-driven pulsating flow. Blythman

et al. [7] examined the driving temperature difference in a rectangular channel under the effect of flow rate pulsations. They concluded that heat transfer would enhance in the second half of the cycle when the flow rate was lower than its average value.

Although considerable research efforts have been devoted to understanding the physics of pulsating Newtonian fluid flow, it is possible to claim that studies on pulsating non-Newtonian fluid flow are limited. Daprà and Scarpi [12] analytically examined the pulsating flow of a power-law fluid in a pipe using the power series expansion method. Edwards et al. [13] obtained velocity distribution of power-law fluid flow in a circular channel under pulsating flow conditions. In the analysis, the frequency, amplitude and power-law index were taken into account to reveal their effects on the velocity profile. It was understood that a reverse flow occurred at low frequency and high amplitude values. Balmer and Fiorina [5] obtained a numerical solution for the pulsating flow of a power-law fluid in a circular tube using an implicit finite difference method. For the same problem, Warsi [24] conducted a numerical study to examine the effects of constant and fluctuating pressure gradients on the velocity profile. Afrouzi et al. [1] examined the effects of power-law indice and Reynolds number on the hydrodynamic characteristics of pulsating non-Newtonian fluid flow in a corrugated channel by using the lattice Boltzmann method and the boundary fitting method. Their results showed that the skin factor was a strong function of power-law index in the laminar flow regime. Moreover, recently, extensive studies have been carried out on the oscillatory flow of nanofluids. In this context, the effects of parameters, such as nanoparticles, shape factor [2, 15, 18], phase angle [15, 17, 18] and frequency [15, 18] on flow, and heat transfer were investigated for different nanofluid types.

The above mentioned literature survey studies also revealed that most of the studies regarding to non-Newtonian pulsating flow have generally focused on the investigation of hydrodynamic characteristics without taking the heat transfer phenomenon into account. However, in many engineering applications involving pulsating flow such as hydraulic systems, respiratory/circulatory systems and artificial organs/veins, an accurate estimation of heat transfer and pressure drop is required for a proper design or optimization. To highlight, in a human body, the blood flow rate and the vessel size may alter as a response to the local temperature level. Therefore, it is necessary to carry out comprehensive studies examining the non-Newtonian fluid flow and heat transfer together under pulsating flow conditions.

It is important to note down that disclosures about the effects of a pulsating flow on heat transfer in the existing literature are generally controversial. It was shown that the time-averaged Nusselt number compared to its steady counterpart did not change, increase or even decrease. Therefore, further studies are needed to explain pertinent mechanisms of pulsating flows involving parameters amplitude, frequency, Reynolds number, etc.

In the scope of this study, the problem of pulsating non-Newtonian fluid flow for a fully developed laminar flow regime in a circular pipe is examined theoretically. In the analysis, frequency, amplitude and power-law index are considered as variable parameters. The constant heat flux thermal boundary condition is applied at the wall of the relevant geometry. The perturbation method based on the series expansion, which allows the solution of linear and/or nonlinear ordinary or partial differential equations, is used.

2 Analysis

Hydrodynamically fully developed pulsating flow of a power-law fluid in a circular pipe held at uniform heat flux is considered (see Fig. 1). Thermophysical properties of the fluid are assumed to be constant, and the axial heat conduction in the fluid wall is assumed to be negligible. The governing conservation equations of momentum [6] and energy [6] are as follows:

$$\rho\frac{\partial u}{\partial t} = -\frac{\partial p}{\partial x} - \frac{1}{r}\frac{\partial(r\tau_{rx})}{\partial r},$$

$$\frac{\partial T}{\partial t} + u\frac{\partial T}{\partial x} = \alpha\frac{1}{r}\frac{\partial}{\partial r}\left(r\frac{\partial T}{\partial r}\right).$$

The symbols appearing in the above set of equations are as follows: p is the pressure; u the axial velocity; T the temperature; t the time; x, r the axial and radial coordinate; τ the shear stress; ρ the density and α the thermal diffusivity, respectively.

The regarding boundary conditions are given below:

$$r = 0: \quad \frac{\partial u}{\partial r} = 0, \quad \frac{\partial T}{\partial r} = 0, \qquad r = r_\circ: \quad u = 0, \quad T = T_w.$$

We assume that the pulsating flow is driven by the pressure gradient, which oscillates with time, as follows:

$$-\frac{\partial p}{\partial x} = P_0\big(1 + \epsilon e^{\imath\omega t}\big),$$

where P_0, ω, ϵ and ω are the pressure gradient, the angular frequency, the amplitude and the frequency of the pressure, respectively.

The constitutive equation, which relates shear stress with shear rate, can be written by using the simple two-parameter power-law model as follows:

$$\tau_{rx} = \eta\left|\frac{\partial u}{\partial r}\right|^{n-1}\frac{\partial u}{\partial r}, \tag{1}$$

where η denotes the consistency index of the fluid, and n is the power-law index giving a measure of the pseudoplasticity with departure from unity showing more pronounced shear-thinning ($n < 1$) or shear-thickening characteristics ($n > 1$). For $n = 1$, the fluid exhibits Newtonian behavior.
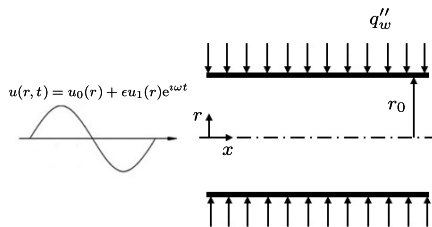
Figure 1. The schematic of the problem geometry.

For a power-law fluid in a pipe, Eq. (1) might be expressed as follows [9]:

$$\tau_{rx} = \eta\left(-\frac{\partial u}{\partial r}\right)^n.\tag{2}$$

The following dimensionless quantities are introduced:

$$R = \frac{r}{r_\circ}, \quad U = \frac{u}{\bar{u}_0}, \quad t^* = \omega t, \quad Re = \frac{\rho\bar{u}_0^{2-n}D_h^n}{\eta}, \quad \tau_w^* = \frac{\tau_w}{\eta}\left(\frac{r_\circ}{\bar{u}_0}\right)^n,$$

$$F = Re\frac{r_\circ\omega}{\bar{u}_0}, \quad \theta = \frac{T - T_w}{(q_w''D_h)/k}, \quad Pr = \frac{\eta c_p}{k}\left(\frac{\bar{u}_0}{r_\circ}\right)^{n-1}, \quad P^* = -\frac{1}{P_0}\frac{\partial p}{\partial x},$$

where $D_h(= 2r_\circ)$ is the hydraulic diameter, R, U, $r_\circ$, Re, F, θ, q'', k, Pr and c_p is the dimensionless radial coordinate, the dimensionless axial velocity, radius of the pipe, Reynolds number, dimensionless frequency, dimensionless temperature, heat flux, thermal conductivity, Prandtl number and specific heat at constant pressure, respectively, $*$ represent dimensionless variable, subscript w is the wall, and $\bar{u}_0$ is the mean velocity defined as follows:

$$\bar{u}_0 = \frac{n}{3n+1}\left(\frac{P_0 r_\circ^{n+1}}{2\eta}\right)^{1/n}.$$

Using the definition of axial temperature gradient for the case of constant heat flux condition

$$\frac{\partial T}{\partial x} = \frac{2q_w''}{\rho c_p \bar{u}(t)r_\circ},$$

the governing equations in a nondimensional form might be written as follows:

$$\frac{F}{2^n}\frac{\partial U}{\partial t^*} = 2\left\{\frac{3n+1}{n}\right\}^n(1 + \epsilon e^{\imath\omega t}) - \frac{1}{R}\frac{\partial}{\partial R}\left(R\left(-\frac{\partial U}{\partial R}\right)^n\right),\tag{3}$$

$$\frac{FPr}{2^n}\frac{\partial\theta}{\partial t^*} + \frac{U(R,t^*)}{\bar{U}(t^*)} = \frac{1}{R}\frac{\partial}{\partial R}\left(R\frac{\partial\theta}{\partial R}\right).\tag{4}$$

Similarly, the corresponding boundary conditions might be obtained as

$$R = 0: \quad \frac{\partial U}{\partial R} = 0, \quad \frac{\partial\theta}{\partial R} = 0, \qquad R = 1: \quad U = 0, \quad \theta = 0.\tag{5}$$

The solution of Eqs. (3) and (4) can be reached by the perturbation method, which is a semianalytical method based on power expansion. Thus, the amplitude ϵ is small, and the solution is obtained to first order of approximation:

$$U(R, t^*) = U_0(R) + \epsilon U_1(R)e^{\imath t^*} + O(\epsilon^2),\tag{6}$$

$$\theta(R, t^*) = \theta_0(R) + \epsilon\theta_1(R)e^{\imath t^*} + O(\epsilon^2).\tag{7}$$

Using binomial expansion, the shear rate in Eq. (2) might be written as follows:

$$\left(-\frac{\partial U}{\partial R}\right)^n = \left(-\frac{dU_0}{dR}\right)^n\left[1 - \epsilon n\frac{dU_1/dR}{-dU_0/dR}e^{\imath t^*} + O(\epsilon^2)\right].\tag{8}$$

After substituting Eqs. (6) and (8) into Eqs. (3) and (5), we can equate terms of identical powers of ϵ. Hence, we have the following equations:

$$0 = 2\left\{\frac{3n+1}{n}\right\}^n - \frac{1}{R}\frac{\mathrm{d}}{\mathrm{d}R}\left(R\left(-\frac{\mathrm{d}U_0}{\mathrm{d}R}\right)^n\right),$$

$$\frac{F\imath}{2^n}U_1 = 2\left\{\frac{3n+1}{n}\right\}^n + \frac{1}{R}\frac{\mathrm{d}}{\mathrm{d}R}\left(R\left[n\left(-\frac{\mathrm{d}U_0}{\mathrm{d}R}\right)^{n-1}\frac{\mathrm{d}U_1}{\mathrm{d}R}\right]\right).$$

The analytical solution for the steady and first-order component of the velocity are obtained as follows:

$$U_0(R) = \frac{3n+1}{n+1}\left[1 - R^{(n+1)/n}\right],$$

$$U_1(R) = -\frac{2\imath(6+\frac{2}{n})^n}{F}\left[1 - \frac{R^{(1-n)/(2n)}J_v\left[\imath cR^{(1+n)/(2n)}\right]}{J_v[\imath c]}\right],$$

where J_v is the Bessel function of the first kind of order v, v and c are the parameter written as

$$v = \frac{n-1}{n+1}, \qquad c^2 = 4F\imath\frac{1+3n}{(1+n)^2}\left(\frac{n}{2+6n}\right)^n.$$

For an unsteady, pressure driven and fully developed pipe flow, the balance of forces acting in the flow direction can be expressed as

$$\pi r_\circ^2 p - \pi r_\circ^2\left(p + \frac{\partial p}{\partial x}\,\mathrm{d}x\right) - 2\pi r_\circ^2\tau_w\,\mathrm{d}x = \rho\pi r_\circ^2\,\mathrm{d}x\frac{\mathrm{d}\bar{u}(t)}{\mathrm{d}t}.$$

This equation can be rearranged to give

$$-\frac{\partial p}{\partial x} = \frac{2}{r_\circ}\tau_w + \rho\frac{\mathrm{d}\bar{u}(t)}{\mathrm{d}t}.$$

According to the Darcy's formula, the relation between the pressure gradient and the friction factor might be defined as

$$\frac{\partial p}{\partial x} = f\frac{\rho}{2D_h}\left(\bar{u}(t)\right)^2.$$

By using the definition of shear stress at the wall

$$\tau_w = \eta\left(-\frac{\partial u}{\partial r}\right)^n\bigg|_{r=r_\circ}$$

the dimensionless friction factor might be rewritten as

$$f\,Re = \frac{1}{[\bar{U}(t^*)]^2}\left[4F\frac{\mathrm{d}\bar{U}(t^*)}{\mathrm{d}t^*} + 2^{n+3}\left(-\frac{\partial U}{\partial R}\right)^n\bigg|_{R=1}\right]. \tag{9}$$

$\bar{U}(t^*)$ is the spatial average of dimensionless velocity given as follows:

$$\bar{U}(t^*) = \frac{\int_0^1 U(R, t^*) R \, \mathrm{d}R}{\int_0^1 R \, \mathrm{d}R} = 1 + \epsilon\beta\mathrm{e}^{\imath t^*}, \tag{10}$$

where I_v and β are the Modified Bessel function of the first kind of order v and coefficient, respectively,

$$\beta = -\frac{2\imath(6 + \frac{2}{n})^n}{F}\left[1 - \frac{4nI_{v+1}[c]}{c(1+n)I_v[c]}\right].$$

Considering Eqs. (9) and (10), the friction factor is obtained as

$$f = f_0 + \epsilon f_1 \mathrm{e}^{\imath t^*}, \tag{11}$$

where f_0 and f_1 might be expressed as follows:

$$f_0 Re = 2^{n+3}\left(-\frac{\mathrm{d}U_0}{\mathrm{d}R}\right)^n\bigg|_{R=1},$$

$$f_1 Re = 4F\imath\beta - 2^{n+4}\beta\left(-\frac{\mathrm{d}U_0}{\mathrm{d}R}\right)^n\bigg|_{R=1} - 2^{n+3}n\left[\left(-\frac{\mathrm{d}U_0}{\mathrm{d}R}\right)^{n-1}\frac{\mathrm{d}U_1}{\mathrm{d}R}\right]_{R=1}.$$

By integrating Eq. (11) over a period, the averaged friction factor might be written as

$$f_{\mathrm{avg}} = \frac{1}{2\pi}\int\limits_0^{2\pi} f \, \mathrm{d}t^*.$$

In a similar way, by substituting Eq. (7) into Eqs. (4), (5) and equating terms of identical powers of ϵ

$$\frac{1}{R}\frac{\mathrm{d}}{\mathrm{d}R}\left(R\left(\frac{\mathrm{d}\theta_0}{\mathrm{d}R}\right)\right) = U_0^*(R), \tag{12}$$

$$\frac{1}{R}\frac{\mathrm{d}}{\mathrm{d}R}\left(R\left(\frac{\mathrm{d}\theta_1}{\mathrm{d}R}\right)\right) = U_1^*(R) + \frac{FPr}{2^n}\imath\theta_1(R), \tag{13}$$

where $U_0^*(R)$ and $U_1^*(R)$ are the components of the ratio of dimensionless velocity to spatial average of $U(R, t^*)$, which is given as

$$\frac{U(R, t^*)}{\bar{U}(t^*)} = \frac{U_0(R) + \epsilon U_1(R)\mathrm{e}^{\imath t^*}}{1 + \epsilon\beta\mathrm{e}^{\imath t^*}} = U_0^*(R) + \epsilon U_1^*(R)\mathrm{e}^{\imath t^*},$$

$$U_0^*(R) = U_0(R), \qquad U_1^*(R) = -\beta U_0^*(R) + U_1(R).$$

Considering the boundary conditions defined in Eqs. (5), (12) can be obtained as

$$\theta_0(R) = \frac{3n+1}{n+1}\left[\frac{R^2-1}{4} - \left(\frac{n}{3n+1}\right)^2\left(R^{(3n+1)/n} - 1\right)\right].$$

The Green's function approach is used to solve Eq. (13) (see Appendix). This function is an effective approach to solve boundary value problems with inhomogeneous ordinary differential equations

$$\theta_1(R) = J_0(AR)\big[I_1(R) + I_3(R)\big] + Y_0(AR)I_2(R),$$

where Y_0 and A are the Bessel function of the second kind of order 0 and parameter, respectively, $A^2 = -F\imath Pr/2^n$,

$$I_1(R) = \int_0^R -\frac{\pi}{2}\frac{J_0(A\xi)Y_0(A)}{J_0(A)}\xi U_1^*(\xi)\,d\xi, \qquad I_2(R) = \int_0^R \frac{\pi}{2}J_0(A\xi)\xi U_1^*(\xi)\,d\xi,$$

$$I_3(R) = \int_R^1 -\frac{\pi}{2}\frac{(J_0(A\xi)Y_0(A) - J_0(A)Y_0(A\xi))}{J_0(A)}\xi U_1^*(\xi)\,d\xi.$$

The dimensionless bulk temperature θ_b is given by

$$\theta_b = \frac{\int_0^1 U\theta R\,dR}{\int_0^1 UR\,dR}.$$

By using the perturbation solutions of dimensionless velocity and temperature, the first order bulk temperature is obtained in the form below:

$$\theta_b = \frac{\int_0^1 (U_0\theta_0 + \epsilon(U_0\theta_1 + U_1\theta_0)e^{\imath t^*})R\,dR}{\frac{1}{2}(1 + \epsilon\beta e^{\imath t^*})}.$$

The Nusselt number, based on the difference between the wall and the bulk temperature, can be defined as

$$Nu = \frac{1}{\frac{T_w - T_b}{q_w'' D_h/k}} = -\frac{1}{\theta_b}.$$

In order to identify the effect of oscillating flow on heat transfer rate, the Nusselt number needs to be written in the following form:

$$Nu = Nu_0 + \epsilon Nu_1 e^{\imath t^*}, \tag{14}$$

where Nu_0 and Nu_1 are the steady and oscillatory components of the Nusselt number, which are given, respectively, as

$$Nu_0 = -\frac{1/2}{\int_0^1 U_0\theta_0 R\,dR}, \qquad Nu_1 = -\frac{\beta/2 + Nu_0\int_0^1 (U_0\theta_1 + U_1\theta_0)R\,dR}{\int_0^1 U_0\theta_0 R\,dR}.$$

By integrating the Eq. (14) over a period, the averaged Nusselt number is obtained as

$$Nu_{\mathrm{avg}} = \frac{1}{2\pi}\int_0^{2\pi} Nu\,dt^*.$$

3 Results and discussion

Fully developed laminar pulsating flow in a circular pipe held at uniform heat flux is investigated considering the power-law model for the working fluid. The interactive effects of power-law index n, amplitude ϵ and frequency F on convective heat transfer are examined. At first, we validated our analysis by comparing some specific results with those available in the existing literature, mainly, by those of Edwards et al. [13] and Nield and Kuznetsov [20].

Edwards et al. [13], as previously emphasized in the literature, examined power-law fluid flow in a circular channel under the pulsating flow conditions. As it can be seen from Fig. 2, the dimensionless velocity distributions obtained for different values of power-law index and phase angle display an excellent agreement with the reference study.

Another literature comparison is made with the study by Nield and Kuznetsov [20] for the Newtonian fluid behavior. Nield and Kuznetsov [20] analytically solved the forced convection problem on the walls of which uniform heat flux thermal boundary condition was applied. The results of the variation of the Nusselt number with dimensionless frequency obtained for different Prandtl number values from both studies are compared in Fig. 3. It is seen that the results are consistent.

(a) $n = 0.7$ (b) $n = 1.0$ (c) $n = 1.4$
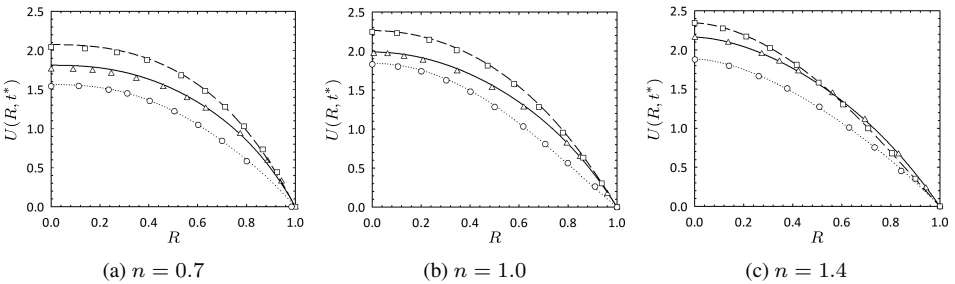
Figure 2. The validation against the results by Edwards et al. [13]. The present study is shown by the hairline, the dashed line and the dotted line for $t^* = 0, 2\pi/5, 8\pi/5$ (a); $t^* = 0, 2\pi/5, 6\pi/5$ (b), $t^* = 0, 4\pi/5, 8\pi/5$ (c), respectively. Edwards et al. [13]: $\triangle, \square, \circ$ for $t^* = 6.0, 6.2, 6.8$ (a); $t^* = 4.0, 4.2, 4.6$ (b); $t^* = 4.0, 4.4, 4.8$ (c), respectively; $\epsilon = 1.0$, $F = 10$.
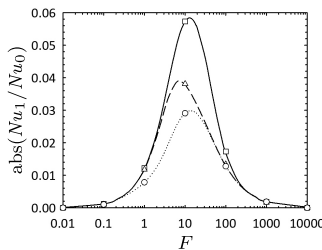
Figure 3. The validation against the results by Nield and Kuznetsov [20]. The present study is shown by the hairline, the dashed line and the dotted line for $Pr = 0.1, 1, 10$, respectively; Nield and Kuznetsov [20]: $\square, \triangle, \circ$ for $Pr = 0.1, 1, 10$, respectively; $n = 1$.

Table 1. Comparison of Nusselt number values with those obtained by Grigull [14].

n	Present	Grigull [14]
0.7	4.53843	4.53843
1	4.36364	4.36364
1.4	4.23625	4.23625
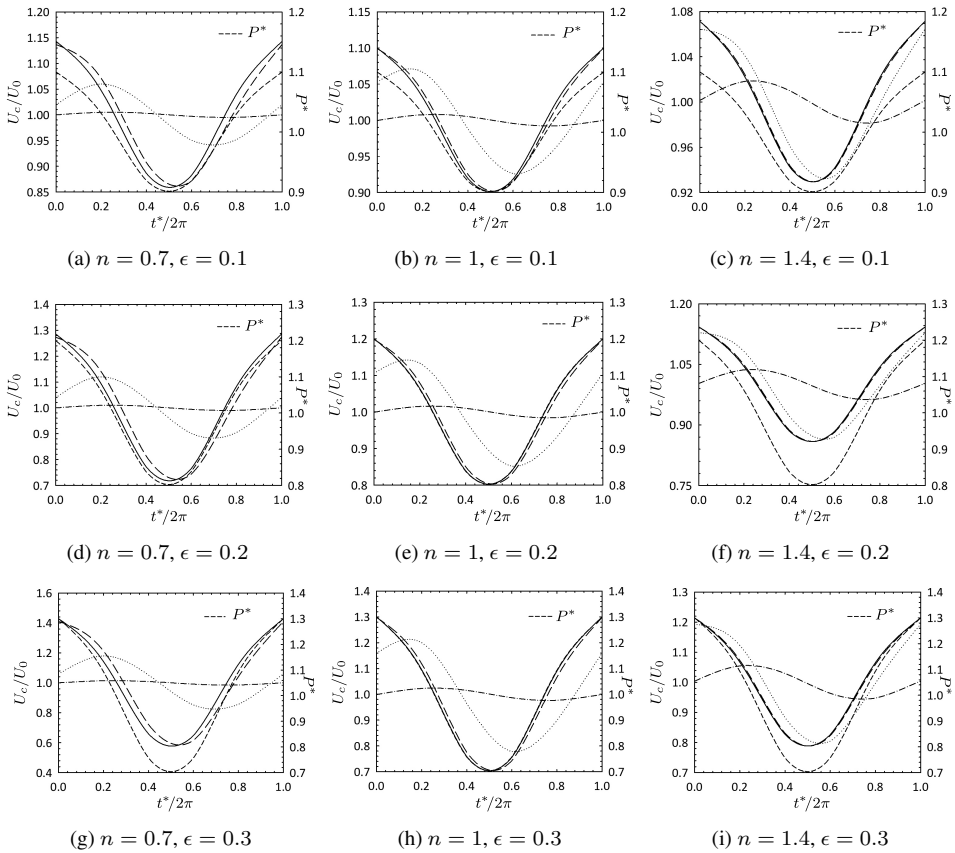
Figure 4. The variation of the dimensionless centerline velocity over a period. The frequency is shown by the hairline, the dashed line, the dotted line and the dash-dotted line for $F = 0.1, 1, 10, 100$, respectively.

For assuring an additional credence to the methodology followed, the Nusselt number value for the power-law fluid flow in a circular pipe with uniform heat flux on the wall at $\epsilon = 0$ are compared with those by Grigull [14]. As seen in Table 1, the results are consistent with those by [14].

Figure 4 shows the variation of dimensionless centerline velocity over a period for a shear-thinning fluid ($n = 0.7$), a Newtonian fluid ($n = 1$) and a shear-thickening fluid ($n = 1.4$), respectively, at different values of the dimensionless frequency F. As can be
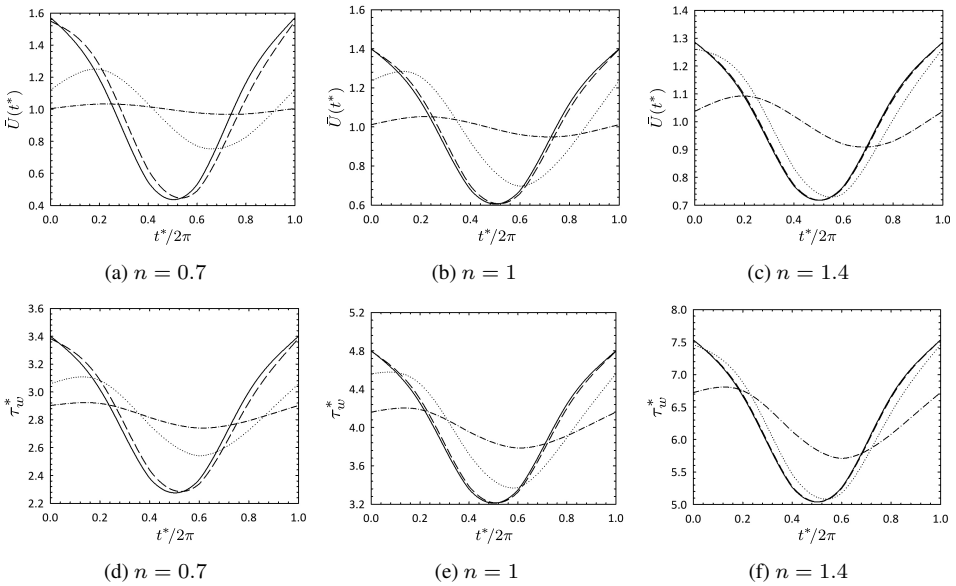
Figure 5. The variations of the spatial average of dimensionless velocity and the wall shear stress for over a period. The frequency is shown by the hairline, the dashed line, the dotted line and the dash-dotted line for $F = 0.1, 1, 10, 100$, respectively; $\epsilon = 0.2$.

seen from these figures, the dimensionless velocity at the center and the applied pressure gradient follow a similar phase for the lowest value of F ($F = 0.1$), which is called quasisteady state [21, 22]. As the dimensionless frequency increases, pulse amplitude of the centerline velocity decreases. As a consequence, maximum points increase, while minimum points are decreasing. Furthermore, with an increase in F, a phase lag is observed for the periodic variation of the dimensionless centerline velocity according to the applied pressure gradient. Increasing amplitude presents similar behaviors.

Similarly, Fig. 5 illustrates the variations of the spatial average of dimensionless velocity and the wall shear stress for over a period for $n = 0.7, 1$ and 1.4, respectively, at different values of the dimensionless frequency F.

In order to discuss the effect of the amplitude ϵ on the friction factor, the variation of fRe over a period at various values of ϵ at $F = 10$ for $n = 0.7, 1, 1.4$ is depicted in Fig. 6. As expected, with increasing ϵ, pulse amplitude of fRe increases. As it is well known, increasing the power-law index leads to an increased friction.

Similarly, Fig. 7 illustrates the change of fRe over a period with varying nondimensional frequency F at $\epsilon = 0.2$ for $n = 0.7, 1, 1.4$. As it is obvious from the figure, the variation of fRe dramatically changes depending on the power-law index n. For the shear-thinning fluid ($n = 0.7$), a phase shift occurs with an increase in F, which is accompanied by a decreased change amplitude (i.e. the highest value of fRe decreases, and its lowest value decreases). For the Newtonian fluid ($n = 1$), the phase shift is again discernible. However, no variation is observed in the variation amplitude with constant
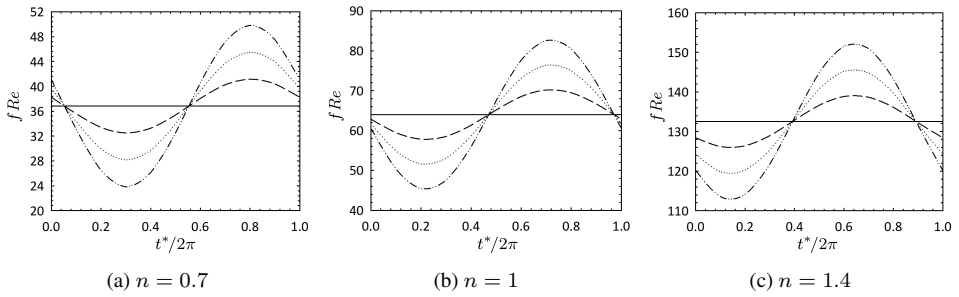
Figure 6. The variation of the fRe over a period for varying amplitudes shown by the hairline, the dashed line, the dotted line and the dash-dotted line when $\epsilon = 0, 0.1, 0.2, 0.3$, respectively; $F = 10$.
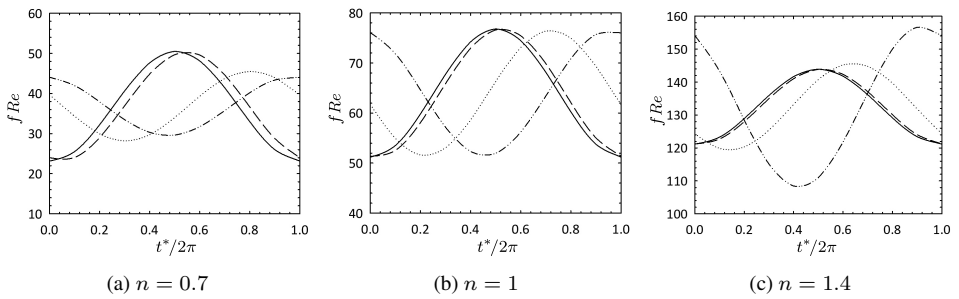
Figure 7. The variation of the fRe over a period for varying frequencies shown by the hairline, the dashed line, the dotted line and the dash-dotted line for $F = 0.1, 1, 10, 100$, respectively; $\epsilon = 0.2$.
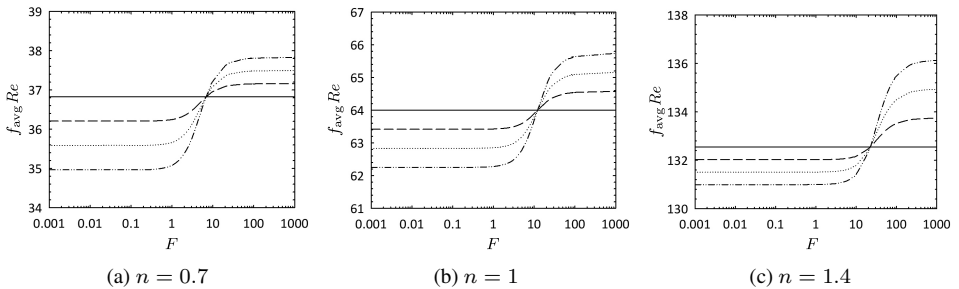
Figure 8. The variations of the $f_{avg}Re$ with F for different values of amplitude shown by the hairline, the dashed line, the dotted line and the dash-dotted line when $\epsilon = 0, 0.1, 0.2, 0.3$, respectively.

maximum and minimum points. For the shear-thinning fluid ($n = 1.4$), the phase shift is still on the scene with increasing F. However, increasing F leads to an increase in the amplitude. This behavior in the friction factor might be attributed to the complex relations among the parameters affecting fRe (see Eq. (9)).

The variation of the averaged friction factor with the dimensionless frequency F at varying values of amplitude for $n = 0.7, 1, 1.4$ is shown in Fig. 8. With an increase in amplitude, the $f_{avg}Re$ decreases up to a certain frequency value, while it increases after

the relevant frequency value. These frequency values are approximately; $F = 6.85$ for the shear thinning fluid ($n = 0.7$), $F = 12.286$ for the Newtonian fluid ($n = 1$) and $F = 22.279$ for the shear thickening fluid ($n = 1.4$), respectively. For $n = 0.7$, $f_{\mathrm{avg}}Re$ is constant for $0 \leqslant F \leqslant 0.659$. Then it increases for the range of $0.659 \leqslant F \leqslant 51.288$, and finally, it again becomes constant for $F \geqslant 51.288$. That means that increasing F is only effective for a specific range of F. For $n = 1$ and $n = 1.4$, similar behaviors are obtained with F-dependent ranges of $1.352 \leqslant F \leqslant 114.48$ and $3.562 \leqslant F \leqslant 266.518$, respectively. Out of these ranges, an F-independent behavior persists. It should be noted that F-dependent range extends with an increase in the power-law index n.

Figure 9 shows the variations of averaged friction factor with the amplitude for $n = 0.7, 1$ and 1.4, respectively, at different values of the dimensionless frequency F. With increasing ϵ, $f_{\mathrm{avg}}Re$ decreases at lower values of F ($F = 0.1$ and 1), while it increased at $F = 100$ for all the fluid types considered ($n = 0.7, 1$ and 1.4). For $F = 10$, an increase in ϵ results in an increase in $f_{\mathrm{avg}}Re$ for $n = 0.7$ and 1, while it results in a decrease for $n = 1.4$.

In order to understand the effects of the dimensionless frequency and the amplitude on heat transfer, dimensionless bulk temperatures are drawn at first. Figures 10, 11 show the variation of the dimensionless bulk temperature and the Nusselt number over a period

(a) $n = 0.7$ (b) $n = 1$ (c) $n = 1.4$
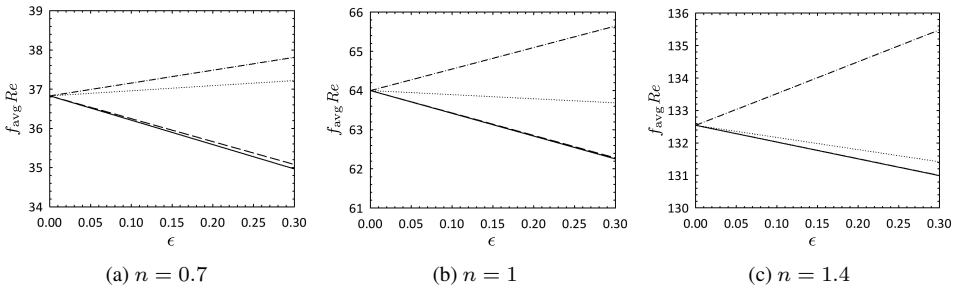
Figure 9. The variation of the $f_{\mathrm{avg}}Re$ with ϵ for different values of frequency shown by the hairline, the dashed line, the dotted line and the dash-dotted line for $F = 0.1, 1, 10, 100$, respectively.

(a) $n = 0.7$, $\epsilon = 0.1$ (b) $n = 1$, $\epsilon = 0.1$ (c) $n = 1.4$, $\epsilon = 0.1$
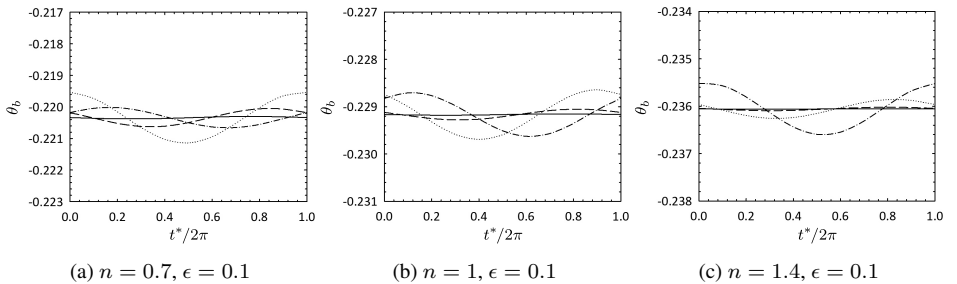
Figure 10. The variation of the dimensionless bulk temperature over a period. The frequency is shown by the hairline, the dashed line, the dotted line and the dash-dotted line for $F = 0.1, 1, 10, 100$, respectively; $Pr = 10$.
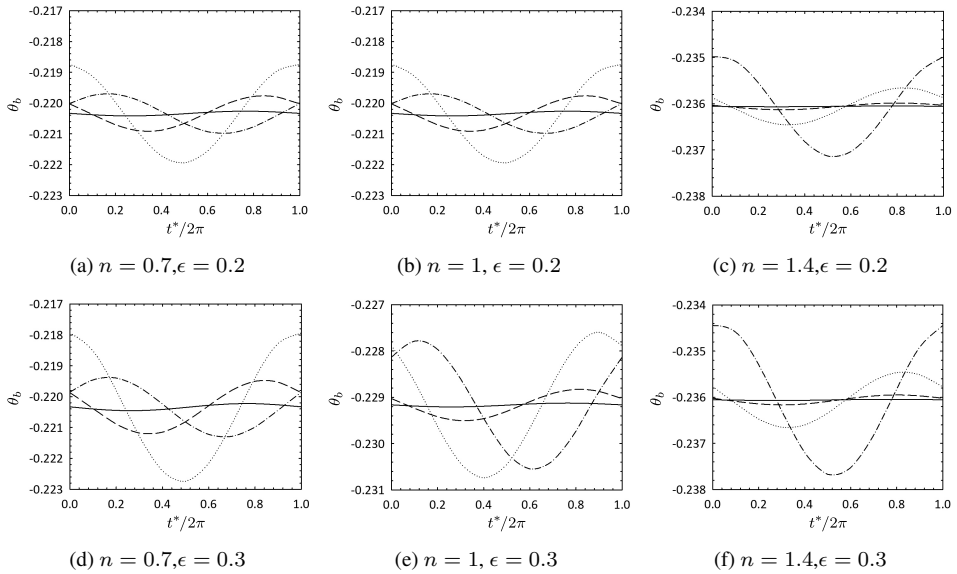
Figure 11. The variation of the dimensionless bulk temperature over a period. The frequency is shown by the hairline, the dashed line, the dotted line and the dash-dotted line for $F = 0.1, 1, 10, 100$, respectively; $Pr = 10$.
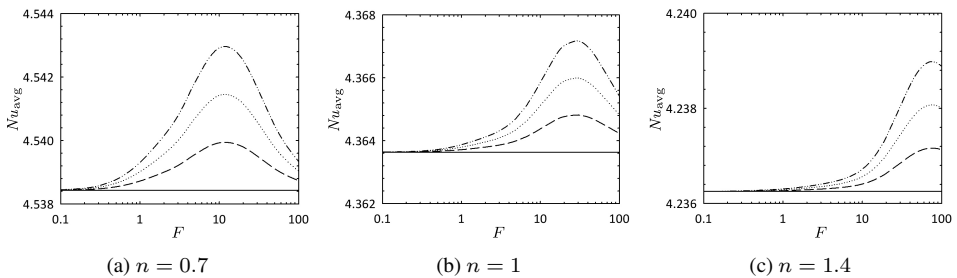
Figure 12. The variation of the averaged Nusselt number with F for different values of amplitude shown by the hairline, the dashed line, the dotted line and the dash-dotted line when $\epsilon = 0, 0.1, 0.2, 0.3$, respectively; $Pr = 10$.

for the shear-thinning fluid ($n = 0.7$), the Newtonian fluid ($n = 1$) and the shear-thickening fluid ($n = 1.4$), respectively.

The variation of the averaged Nusselt number with the dimensionless frequency F at varying values of amplitude for $n = 0.7, 1$ and 1.4 is depicted in Fig. 12. It is observed that with an increase in the amplitude, the averaged Nusselt number increases for all the fluid types considered. With increasing F, Nu_{avg} increases up to a critical value of F, then it decreases. This critical value for F is $11.708, 28.349$ and 76.268 for $n = 0.7, 1$ and 1.4, respectively, which is interestingly independent of the amplitude ϵ. A similar behavior is also noted in [20] for the case of pulsatile flow of Newtonian fluid flow in both circular tube and parallel-plates channels.

4   Conclusions

As a breakthrough attempt, the pulsating Newtonian and non-Newtonian fluid flows in
a circular pipe have been studied for the fully developed flow condition. A perturbation se-
ries method has been used in the analysis. The working parameters were the frequency F,
the amplitude ϵ, and the power-law index n. Their interactive effects on the Nusselt
number as well as the friction factor have been identified. The major findings of the
present study might be summarized as follows:

- As the dimensionless frequency increases, a phase lag is observed for the periodic
  variation of the dimensionless velocity at center according to the applied pressure
  gradient.
- The dimensionless frequency is effective on the friction factor for its specific range.
  The spectrum of this range enlarges with an increase in the power-law index.
- The effect of the amplitude on the friction factor changes according to F.
- With an increase in the dimensionless frequency, the averaged Nusselt number is
  observed to increase up to a critical value of F, which decreases afterwards. This
  critical value tends to increase with the power-law index, which is interestingly
  independent of the amplitude ϵ.

Appendix

Writing the Green's function in the $G(R, \xi)$ form for Eq. (13):

$$\frac{1}{R}\frac{\mathrm{d}}{\mathrm{d}R}\left(R\left(\frac{\mathrm{d}G(R,\xi)}{\mathrm{d}R}\right)\right) + A^2 G(R,\xi) = \delta(R - \xi), \tag{A.1}$$

where $\delta(R - \xi)$ is the Dirac delta function.

Similarly, the boundary conditions defined in Eq. (5) can be given as

$$R = 0: \quad \frac{\partial G}{\partial R} = 0, \qquad R = 1: \quad G = 0. \tag{A.2}$$

In the light of this knowledge, the general solution of Eq. (A.1) is obtained as follows:

$$G(R, \xi) = \begin{cases} c_{11} J_0(AR) + c_{12} Y_0(AR), & 0 \leqslant R < \xi, \\ c_{21} J_0(AR) + c_{22} Y_0(AR), & \xi < R \leqslant 1, \end{cases} \tag{A.3}$$

where c_{ij}'s are functions that depend on ξ. Using the boundary conditions defined in
Eq. (A.2) and the Green's function technique, c_{ij}'s are written as

$$c_{11} = -\frac{\pi}{2}\xi\left[\frac{J_0(A\xi)Y_0(A) - Y_0(A\xi)J_0(A)}{J_0(A)}\right], \qquad c_{12} = 0, \tag{A.4}$$

$$c_{21} = -\frac{\pi}{2}\xi\left[\frac{J_0(A\xi)Y_0(A)}{J_0(A)}\right], \qquad c_{22} = \frac{\pi}{2}\xi J_0(A\xi). \tag{A.5}$$

By substituting Eqs. (A.4)–(A.5) into Eq. (A.3), $G(R, \xi)$ is rearranged as

$$G(R, \xi) = \begin{cases} -\frac{\pi}{2}\xi \frac{J_0(AR)}{J_0(A)}(J_0(A\xi)Y_0(A) - J_0(A)Y_0(A\xi)), & 0 \leqslant R < \xi, \\ -\frac{\pi}{2}\xi \frac{J_0(A\xi)}{J_0(A)}(J_0(AR)Y_0(A) - J_0(A)Y_0(AR)), & \xi < R \leqslant 1. \end{cases}$$

Thus, the solution of Eq. (13) depending on the Green's function is obtained as follows:

$$\theta_1(R) = \int\limits_0^1 G(\xi, R)U_1^*(\xi)\,\mathrm{d}\xi.$$

References

1. H.H. Afrouzi, M. Ahmadian, A. Moshfegh, D. Toghraie, A. Javadzadegan, Statistical analysis of pulsating non-Newtonian flow in a corrugated channel using Lattice-Boltzmann method, *Physica A*, **535**:122486, 2019, https://doi.org/10.1016/j.physa.2019.122486.

2. N.S. Akbar, Z. Iqbal, B. Ahmad, E.N. Maraj, Mechanistic investigation for shape factor analysis of SiO_2/MoS_2-ethylene glycol inside a vertical channel influenced by oscillatory temperature gradient, *Can. J. Phys.*, **97**(9):950–958, 2019, https://doi.org/10.1139/cjp-2018-0717.

3. C. Aygun, O. Aydin, Hydrodynamics of piston-driven laminar pulsating flow: Part 1. Developing flow, *Nucl. Eng. Des.*, **274**:164–171, 2014, https://doi.org/10.1016/j.nucengdes.2014.02.017.

4. C. Aygun, O. Aydin, Hydrodynamics of piston-driven laminar pulsating flow: Part 2. Fully developed flow, *Nucl. Eng. Des.*, **274**(6):172–180, 2014, https://doi.org/10.1016/j.nucengdes.2014.02.018.

5. R.T. Balmer, M.A. Fiorina, Unsteady flow of an inelastic power-law fluid in a circular tube, *J. Non-Newtonian Fluid Mech.*, **7**(2-3):189–198, 1980, https://doi.org/10.1016/0377-0257(80)85005-1.

6. R.B. Bird, W.E. Stewart, E.N. Lightfoot, *Transport Phenomena*, Wiley, New York, 1960.

7. R. Blythman, T. Persoons, N. Jeffers, D.B. Murray, Heat transfer of laminar pulsating flow in a rectangular channel, *Int. J. Heat Mass Transfer*, **128**:279–289, 2019, https://doi.org/10.1016/j.ijheatmasstransfer.2018.08.109.

8. M.O. Carpinlioglu, M.Y. Gundogdu, A critical review on pulsatile pipe flow studies directing towards future research topics, *Flow Meas. Instrum.*, **12**(3):163–174, 2001, https://doi.org/10.1016/S0955-5986(01)00020-6.

9. R.P. Chhabra, J.F. Richardson, *Non-Newtonian Flow and Applied Rheology: Engineering Applications*, Elsevier, Amsterdam, 2008.

10. H.W. Cho, J.M. Hyun, Numerical solution of pulsating flow and heat transfer characteristics in a pipe, *Int. J. Heat Fluid Flow*, **11**(4):321–330, 1990, https://doi.org/10.1016/0142-727X(90)90056-H.

11. O.I. Craciunescu, S.T. Clegg, Pulsatile blood flow effects on temperature distribution and heat transfer in rigid vessels, *J. Biomech. Eng.*, **123**(5):500–505, 2001, `https://doi.org/10.1115/1.1392318`.

12. I. Daprà, G. Scarpi, Pulsatile pipe flow of pseudoplastic fluids, *Meccanica*, **41**(5):501–508, 2006, `https://doi.org/10.1007/s11012-006-0007-6`.

13. T. Edwards, D.A. Nellist, W.L. Wilkinson, Unsteady, laminar flows of non-Newtonian fluids in pipes, *Chem. Eng. Sci.*, **27**(2):295–306, 1971, `https://doi.org/10.1016/0009-2509(72)85066-8`.

14. U. Grigull, Warmeubergang an nicht-Newtonsche Flussigkeiten bei laminarer Rohrstromung, *Chem. Ing. Tech.*, **28**(8–9):553–556, 1956, `https://doi.org/10.1002/cite.330280808`.

15. Z. Iqbal, N.S. Akbar, E. Azhar, E.N. Maraj, Performance of hybrid nanofluid (Cu-CuO/water) on MHD rotating transport in oscillating vertical channel inspired by Hall current and thermal radiation, *Alexandria Eng. J.*, **57**(3):1943–1954, 2018, `https://doi.org/10.1016/j.aej.2017.03.047`.

16. Z.X. Li J.C. Yu, T.S. Zhao, Analytical study of pulsating laminar heat convection in a circular tube with constant heat flux, *Int. J. Heat Mass Transfer*, **47**(24):5297–5301, 2004, `https://doi.org/10.1016/j.ijheatmasstransfer.2004.06.029`.

17. E.N. Maraj, N.S. Akbar, Z. Iqbal, E. Azhar, Framing the mhd mixed convective performance of cnts in rotating vertical channel inspired by thermal deposition: Closed form solutions, *J. Mol. Liq.*, **233**:334–343, 2017, `https://doi.org/10.1016/j.molliq.2017.03.041`.

18. E.N. Maraj, I. Zehra, N. SherAkbar, Rotatory flow of MHD $(MoS_2\text{-}SiO_2)/H_2O$ hybrid nanofluid in a vertical channel owing to velocity slip and thermal periodic conditions, *Colloids Surf., A*, **639**:128383, 2022, `https://doi.org/10.1016/j.colsurfa.2022.128383`.

19. T. Moschandreou, M. Zamir, Heat transfer in a tube with pulsating flow and constant heat flux, *Int. J. Heat Mass Transfer*, **40**(10):2461–2466, 1997, `https://doi.org/10.1016/S0017-9310(96)00266-9`.

20. D.A. Nield, A.V. Kuznetsov, Forced convection with laminar pulsating flow in a channel or tube, *Int. J. Therm. Sci.*, **46**(6):551–560, 2007, `https://doi.org/10.1016/j.ijthermalsci.2006.07.011`.

21. M. Ohmi, M. Iguchi, T. Usui, Flow pattern and frictional losses in pulsating pipe flow. Part 5: Wall shear stress and flow pattern in a laminar flow, *Bull. JSME*, **24**(187):75–81, 1981, `https://doi.org/10.1299/jsme1958.24.75`.

22. R. Siegel, M. Perlmutter, Heat transfer for pulsating laminar duct flow, *J. Heat Transfer*, **84**:111–123, 1962, `https://doi.org/10.1115/1.3684307`.

23. S. Uchida, The pulsating viscous flow superimposed on the steady laminar motion of incompressible fluid in a circular pipe, *Z. Angew. Math. Phys.*, **7**:403–422, 1956, `https://doi.org/doi.org/10.1007/BF01606327`.

24. Z.U.A. Warsi, Unsteady flow of power-law fluids through circular pipes, *J. Non-Newtonian Fluid Mech.*, **55**(2):197–202, 1994, `https://doi.org/10.1016/0377-0257(94)80005-7`.

25. J.R. Womersley, Method for the calculation of velocity, rate of flow and viscous drag in arteries when the pressure gradient is known, *J. Physiol.*, **127**(3):553–563, 1955, `https://doi.org/10.1113/jphysiol.1955.sp005276`.

26. B.H. Yan, L. Yu, Y.H. Yang, Forced convection with laminar pulsating flow in a tube, *Heat Mass Transfer*, **47**(2):197–202, 2011, `https://doi.org/10.1007/s00231-010-0700-9`.